

Role of isospin composition in low-energy nuclear fusionRichard Gumbel,^{1,*} Christian Ross,^{2,†} and A. S. Umar^{2,‡}¹*Department of Life and Physical Sciences, Fisk University, Nashville, Tennessee 48823, USA*²*Department of Physics and Astronomy, Vanderbilt University, Nashville, Tennessee 37235, USA*

(Received 28 July 2023; accepted 5 October 2023; published 14 November 2023)

We employ a microscopic approach that examines the impact of isospin dynamics on the process of low-energy nuclear fusion along an isotope chain and dependence on deformation. Our method utilizes the density constrained time-dependent Hartree-Fock theory (DC-TDHF), where isoscalar and isovector characteristics of the energy density functional (EDF) are examined in turn. This approach is applied to a series of fusion interactions of ¹⁷⁶Yb with increasingly neutron rich isotopes of calcium. By evaluating the contributions from the isoscalar and isovector components of the EDF, we look to quantify the influence of isospin composition on the conditions under which fusion is most likely to take place. Our findings reveal that, in nonsymmetric systems, the isovector dynamics plays a significant role. Its typical effect is a reduction in the potential barrier, which turns into enhancement for neutron-rich systems.

DOI: [10.1103/PhysRevC.108.L051602](https://doi.org/10.1103/PhysRevC.108.L051602)

The study of fusion reactions is one of the major research areas of low-energy heavy-ion physics [1–3]. Unfortunately, from the theoretical standpoint the lack of a practical many-body approach for sub-barrier tunneling requires the reduction of fusion studies to the determination of an effective ion-ion interaction potential that allows for traditional tunneling methods to be employed. If the ion-ion potential is initially computed with frozen nuclear densities other quantal effects, such as the excitation of the target and projectile and transfer of nucleons during the initial phase of the collision, have to be included via various approximations. The most commonly used method to achieve these goals is the coupled-channels (CC) approach [4–6]. An alternate approach, in which the dynamics of the collision is included at the mean-field level, is provided by the density-constrained time-dependent Hartree-Fock (DC-TDHF) method [7,8].

The dependence of fusion cross sections on neutron excess, or specifically the total isospin quantum number $T_z = (Z - N)/2$, is a significant question in the realm of fusion reactions, particularly fusion reactions involving exotic neutron-rich nuclei. This topic has gained further relevance as rare isotope facilities conduct increasingly sophisticated exotic beam experiments [9]. Furthermore, understanding the impact of isospin dynamics on fusion is crucial for the synthesis of superheavy elements using neutron-rich nuclei [10]. Beyond its implications for nuclear structure and reactions, addressing this inquiry holds substantial importance for our comprehension of the nuclear equation of state (EOS) and symmetry

energy [11,12], which are intimately related to nuclear structure [13] and dynamics [14,15], as well as most astrophysical phenomena [16,17]. Typically, the influence of isospin flow during heavy-ion reactions is discussed in terms of the (N/Z) asymmetry of the target and projectile or the Q values associated with nucleon transfer [18]. However, there are still unresolved issues with the Q -value based transfer methods. First, the precise magnitude of fusion enhancement based on a known Q value is not well understood [19,20]. Second, for exotic nuclei Q values may not be available. Finally, the Q -value transfer is based on the entrance channel properties of the participating nuclei whereas the dynamics during the neck formation phase of the collision may introduce other dynamical effects. One such effect, the Pauli exclusion principle, has been recently discussed [21,22]. For reactions involving deformed nuclei the ion-ion barrier and the fusion dynamics also depend on the orientation of the nuclei with respect to the beam axis [23–25].

The time-dependent Hartree-Fock (TDHF) method supplemented with a density constraint, DC-TDHF, takes advantage of the dynamics included in the TDHF time evolution, which has been successfully utilized to study multinucleon transfer reactions [26–30], deep-inelastic damped collisions [31–33], and quasifission [34–41]. The benefit of this approach is that both the structure and reactions are handled on the same footing through an energy density functional with pre-determined parameters. Hence, the dynamical transfer mechanism, and their influence on the ion-ion interaction potentials at the mean-field level can be studied without making *a priori* assumptions.

Within the TDHF theory, the totally antisymmetric many-body wave function is assumed to be a single Slater determinant. Neglecting the two-body correlations preserves the Slater determinant nature of the many-body state throughout the time evolution. This many-body state is then used

* richard.gumbel@vanderbilt.edu; Present address: Facility for Rare Isotope Beams, Michigan State University, East Lansing, Michigan 48824, USA.

† christian.ross@vanderbilt.edu

‡ umar@compSci.cas.vanderbilt.edu

to construct the time-dependent action using an effective nucleon-nucleon interaction. Variation of this action with respect to single-particle states ϕ_λ^* ,

$$\frac{\delta S}{\delta \phi_\lambda^*} = \frac{\delta}{\delta \phi_\lambda^*} \int dt \langle \Phi(t) | H - i\hbar \frac{\partial}{\partial t} | \Phi(t) \rangle = 0, \quad (1)$$

gives us the most probable reaction path as a set of fully microscopic, coupled, nonlinear, self-consistent, time-dependent Hartree-Fock equations of motion for the single-particle states,

$$h(\{\phi_\mu\}) \phi_\lambda(r, t) = i\hbar \frac{\partial}{\partial t} \phi_\lambda(r, t) \quad (\lambda = 1, \dots, A), \quad (2)$$

where h is the single-particle Hamiltonian. Employing an effective interaction such as the Skyrme interaction results in the total energy of the system being represented as an volume integral of an energy density functional [42],

$$E = \int d^3\mathbf{r} \mathcal{H}(\mathbf{r}). \quad (3)$$

For the purposes of this work the Skyrme EDF may be decomposed into isoscalar and isovector parts [43] (in addition to the conventional kinetic and Coulomb terms) as

$$\mathcal{H}(\mathbf{r}) = \frac{\hbar^2}{2m} \tau_0 + \mathcal{H}_0(\mathbf{r}) + \mathcal{H}_1(\mathbf{r}) + \mathcal{H}_C(\mathbf{r}). \quad (4)$$

The isoscalar and isovector terms carry an isospin index $I = 0, 1$ for the energy densities, respectively. The isoscalar $[\mathcal{H}_0(\mathbf{r})]$ energy density depends on the isoscalar particle density, $\rho_0 = \rho_n + \rho_p$, whereas the isovector $[\mathcal{H}_1(\mathbf{r})]$ energy density depends on the isovector particle density, $\rho_1 = \rho_n - \rho_p$. These definitions, of course, prescribe analogous expressions for other densities and currents. The local gauge and Galilean invariant form is given by [43]

$$\begin{aligned} \mathcal{H}_I(\mathbf{r}) = & C_I^\rho \rho_I^2 + C_I^s s_I^2 + C_I^{\Delta\rho} \rho_I \Delta\rho_I \\ & + C_I^{\Delta s} \mathbf{s}_I \cdot \Delta\mathbf{s}_I + C_I^T (\rho_I \tau_I - \mathbf{j}_I^2) + C_I^T (\mathbf{s}_I \cdot \mathbf{T}_I - \tilde{J}_I^2) \\ & + C_I^{VJ} (\rho_I \nabla \cdot \mathbf{J}_I + \mathbf{s}_I \cdot (\nabla \times \mathbf{j}_I)). \end{aligned} \quad (5)$$

The density dependence of the coupling constants has been restricted to the C_I^ρ and C_I^s terms only, which stems from the most common choice of Skyrme EDF. These density dependent coefficients contribute to the coupling of isoscalar and isovector fields in the Hartree-Fock Hamiltonian [43].

The decomposition of the Skyrme EDF into isoscalar and isovector components makes it feasible to study isospin dependence of nuclear properties microscopically, both for nuclear reactions [44,45] as well as for nuclear structure [43]. This is possible for any approach that employs the Skyrme EDF to compute ion-ion interaction potentials. Here, we implement the decomposed Skyrme EDF in the density-constrained DC-TDHF method [7,45] to study isospin effects in fusion barriers. The DC-TDHF approach permits the study of sub-barrier fusion through the direct calculation of nucleus-nucleus potentials, $V(R)$, from TDHF dynamics. The DC-TDHF method has been used in the study of fusion for a wide range of nuclear reactions [46–52]. The basic idea of the DC-TDHF method is the following: At certain time steps

t [or internucleon distances $R(t)$], a minimization of the static energy is performed while proton and neutron densities are constrained to be the instantaneous densities yielded from the TDHF equations. That is,

$$\begin{aligned} E_{\text{DC}}(R) = & \left\{ E[\rho_n, \rho_p] + \int d^3r \lambda_n(\mathbf{r}) [\rho_n(\mathbf{r}) - \rho_n^{\text{tdhf}}(\mathbf{r}, t)] \right. \\ & \left. + \int d^3r \lambda_p(\mathbf{r}) [\rho_p(\mathbf{r}) - \rho_p^{\text{tdhf}}(\mathbf{r}, t)] \right\} \Big|_{\min_p}, \end{aligned} \quad (6)$$

where $\lambda_n(\mathbf{r})$ and $\lambda_p(\mathbf{r})$ are Lagrange multipliers. This minimized energy is referred to as the so-called density constrained energy, $E_{\text{DC}}(R)$. In essence, all excitation energy has been removed from the system through this procedure. To obtain the underlying ion-ion interaction potential, $V(R)$, the constant binding energies (obtained from a static Hartree-Fock approach) of the two individual nuclei (E_{A_1} and E_{A_2}) are then subtracted:

$$V_{\text{total}}(R) = E_{\text{DC}}(R) - E_{A_1} - E_{A_2}. \quad (7)$$

Ion-ion interaction barriers calculated from the DC-TDHF approach self-consistently contain all of the dynamical changes in the nuclear density throughout the TDHF reaction. Utilizing the decomposition of the Skyrme EDF [Eq. (5)], we can rewrite this potential as

$$V_{\text{total}}(R) = \sum_{I=0,1} v_I(R) + V_{\text{coul}}(R), \quad (8)$$

where $v_I(R)$ denotes the potential computed by using the isoscalar and isovector parts of the Skyrme EDF given in Eqs. (4) and (7). The Coulomb potential is solved from the typical three-dimensional Poisson equation (where the Slater approximation is used for the Coulomb exchange term) via fast Fourier transform techniques.

We have implemented the DC-TDHF approach to study fusion barriers for a number of systems involving spherical isotopes of calcium without the use of the pairing interaction (in particular, calcium-40, -44, -48, and -54) on prolate-deformed ytterbium-176, which permits us to also inspect the orientation dependence of isospin flow. All calculations were done on a three-dimensional Cartesian lattice with no symmetry assumptions [53], and the Skyrme SLy4d EDF [54] was used. The Cartesian box size utilized for all calculations was chosen to be $60 \times 32 \times 32 \text{ fm}^3$, with a mesh spacing of 1.0 fm in all directions. Employing an advanced numerical discretization technique known as the basis-spline collocation method [55], these values provide very accurate numerical results.

For each system under consideration, separate DC-TDHF calculations were performed for two orientations of the prolate-deformed ^{176}Yb nucleus: Euler angle rotations corresponding to $\beta = 0^\circ$ and $\beta = 90^\circ$ (solid and dashed lines, respectively). The center-of-mass energy was chosen to be 1.05 times the corresponding Bass barrier for each system. We begin with fusion of $^{40}\text{Ca} + ^{176}\text{Yb}$ colliding at $E_{\text{c.m.}} = 166.45 \text{ MeV}$, plotted in Fig. 1. The black curves denote the total DC-TDHF potential while the red curves are the combination of isoscalar and Coulomb potentials. The difference

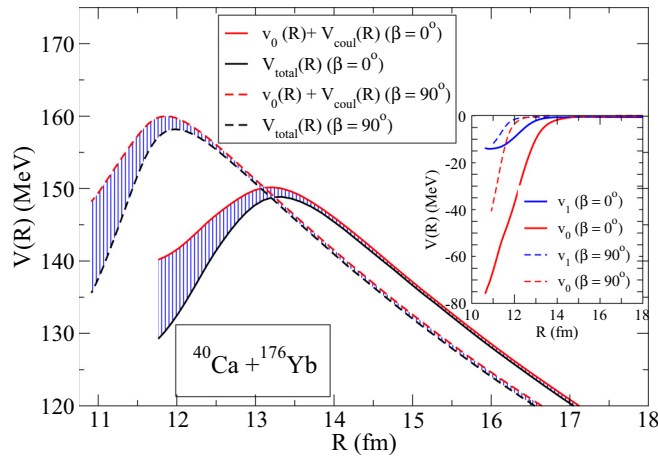


FIG. 1. For the $^{40}\text{Ca} + ^{176}\text{Yb}$ system, total and isoscalar DC-TDHF potentials for two orientations of the prolate-deformed ^{176}Yb (dashed lines denote a Euler angle rotation of $\beta = 90^\circ$). The shaded region in blue depicts a significant *reduction* as an effect of the isovector contribution to the energy density. The inset shows the isoscalar and isovector contributions to the interaction barrier without the Coulomb potential. The TDHF collision energy was $E_{c.m.} = 166.45$ MeV.

between these curves shows the net isovector contribution to the ion-ion interaction potential (shaded regions). For the symmetric, doubly magic ^{40}Ca nucleus colliding with either orientation of ^{176}Yb , there is a substantial reduction of the barrier (area shaded in blue) as a result of the added isovector potentials. This we refer to as the *isovector reduction*, meaning that the isovector contribution is making the overall potential thinner in the inner barrier region and causing a slightly lower barrier height. The inset graph shows

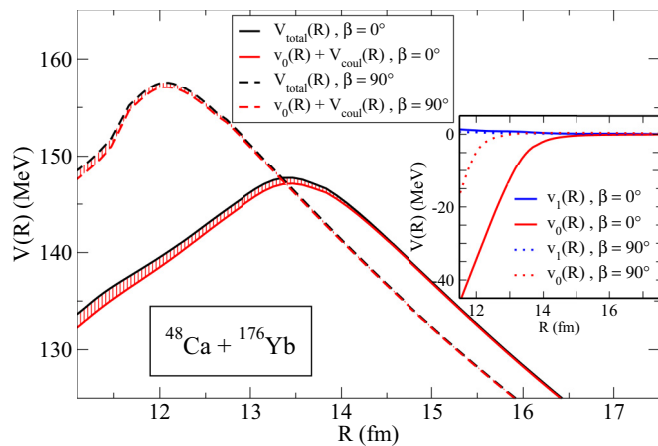


FIG. 2. For the $^{48}\text{Ca} + ^{176}\text{Yb}$ system, total and isoscalar DC-TDHF potentials for two orientations of the prolate-deformed ^{176}Yb (dashed lines denote a Euler angle rotation of $\beta = 90^\circ$). The shaded region in red depicts a small *enhancement* as an effect of the isovector contribution to the energy density. The inset shows the isoscalar and isovector contributions to the interaction barrier without the Coulomb potential. The TDHF collision energy was $E_{c.m.} = 161$ MeV.

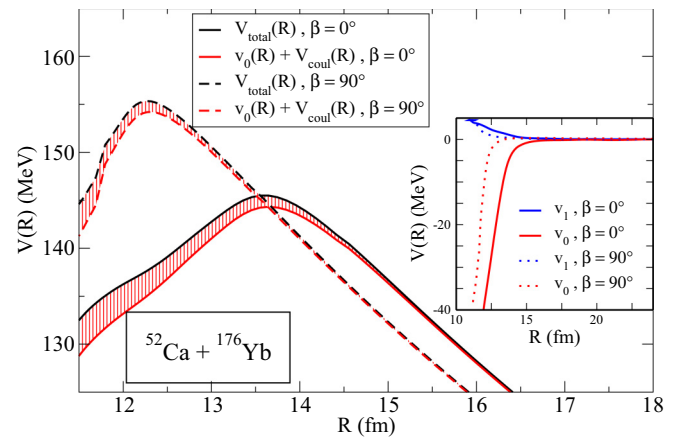


FIG. 3. For the $^{52}\text{Ca} + ^{176}\text{Yb}$ system, total and isoscalar DC-TDHF potentials for two orientations of the prolate-deformed ^{176}Yb (dashed lines denote a Euler angle rotation of $\beta = 90^\circ$). The shaded region in red depicts a significant *enhancement* as an effect of the isovector contribution to the energy density. The inset shows the isoscalar and isovector contributions to the interaction barrier without the Coulomb potential. The TDHF collision energy was $E_{c.m.} = 159.9$ MeV.

the isoscalar/isovector potential contributions by themselves, without the Coulomb energy.

Next, we examine the $^{48}\text{Ca} + ^{176}\text{Yb}$ system at $E_{c.m.} = 161$ MeV. In Fig. 2, with the addition of eight neutrons to the system, we start to see the role of the isovector contribution to the energy density change. Rather than the reduction observed in with ^{40}Ca , there is now a small *isovector enhancement* of the potential barrier (areas shaded in red). This difference in potential barriers for ^{40}Ca and ^{48}Ca is analogous to the

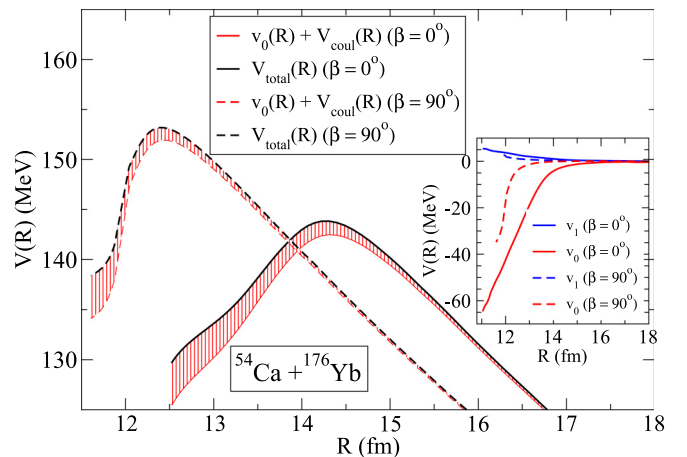


FIG. 4. For the $^{54}\text{Ca} + ^{176}\text{Yb}$ system, total and isoscalar DC-TDHF potentials for two orientations of the prolate-deformed ^{176}Yb (dashed lines denote a Euler angle rotation of $\beta = 90^\circ$). The shaded region in red depicts an even more significant *enhancement* as an effect of the isovector contribution to the energy density. The inset shows the isoscalar and isovector contributions to the interaction barrier without the Coulomb potential. The TDHF collision energy was $E_{c.m.} = 158.98$ MeV.

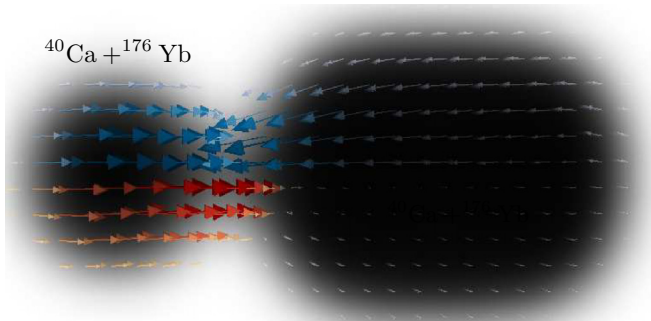


FIG. 5. For the $^{40}\text{Ca} + ^{176}\text{Yb}$ system, single-particle currents for neutrons (upper half slice shown in blue) and for protons (lower half slice shown in red). For this system we observe that the net neutron flow is from ^{176}Yb to ^{40}Ca , while the proton flow is in the opposite direction. Also shown is the shaded outline of the position of the two nuclei (in this case for the $\beta = 0^\circ$ orientation of ^{176}Yb).

experimental observation of a sub-barrier fusion enhancement in the system $^{132}\text{Sn} + ^{40}\text{Ca}$ as compared to the more neutron-rich system $^{132}\text{Sn} + ^{48}\text{Ca}$ [56]. It was shown in an earlier publication [57] that for most systems isovector dynamics results in the thinning of the barrier, thus enhancing the sub-barrier fusion cross sections. The isovector reduction effect vanishes for symmetric systems as well as the $^{48}\text{Ca} + ^{132}\text{Sn}$ system for which neutron pickup Q values are all negative. This enhancement effect becomes more pronounced as further neutrons are introduced to the calcium nuclei. For $^{52}\text{Ca} + ^{176}\text{Yb}$ at $E_{\text{c.m.}} = 159.9$ MeV (Fig. 3) and then $^{54}\text{Ca} + ^{176}\text{Yb}$ at $E_{\text{c.m.}} = 158.98$ MeV (Fig. 4), the potentials calculated from solely the isoscalar and Coulomb terms are now both lower in peak energy, and smaller in width than those calculated with the total density functional.

In all the reactions studied here, we also note that the effect of the isovector contribution is more enhanced for the tip orientation ($\beta = 0$) of the target nucleus. This is likely due to the fact that the contact with the tip orientation happens earlier (larger R) compared to the side orientation. Since the side orientation normally would have a larger area of contact with the projectile, this suggests a competition between time spent between the two nuclei prior to fusion and the size of the overlap region. Thus, nucleon transfer should also depend on the orientation for deformed nuclei, which is normally not taken into account in nonmicroscopic approaches. It is possible to provide a further insight to these results by examining the transfer of neutrons and protons during the contact phase of the collision process since the isovector contribution is intimately related to transfer properties. For this purpose we have plotted the single-particle currents during the TDHF evolution. In Fig. 5 we plot these currents at the initial contact phase for the $^{40}\text{Ca} + ^{176}\text{Yb}$ system, together with the shaded

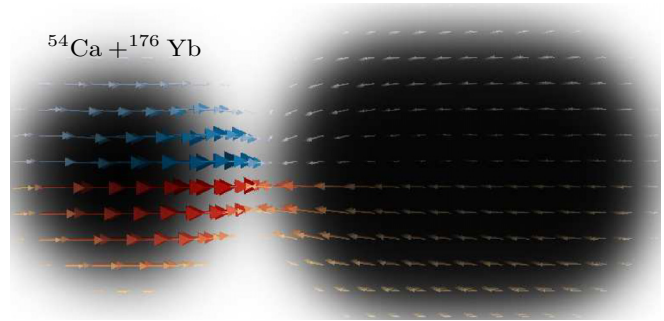


FIG. 6. For the $^{54}\text{Ca} + ^{176}\text{Yb}$ system, single-particle currents for neutrons (upper half slice shown in blue) and for protons (lower half slice shown in red). For this system we observe that the net neutron and proton flow is from ^{54}Ca to ^{176}Yb . Also shown is the shaded outline of the position of the two nuclei (in this case for the $\beta = 0^\circ$ orientation of ^{176}Yb).

outline of the position of the two nuclei (in this case for the $\beta = 0^\circ$ orientation of ^{176}Yb). The upper half plane shows the direction of neutron flow (blue arrows) while the lower half plane shows the proton currents (red arrows). We observe that in this case neutrons are flowing from ^{176}Yb towards ^{40}Ca , while the proton flow is in the reverse direction from ^{40}Ca towards ^{176}Yb . This mode of transfer leads to the isovector reduction of the potential barrier. In Fig. 6 we plot the same quantities for the $^{54}\text{Ca} + ^{176}\text{Yb}$ system. In this case we observe that both neutrons and protons are flowing from ^{54}Ca to ^{176}Yb . The case for ^{52}Ca is similar to the ^{54}Ca and for the ^{48}Ca the net transfer is negligibly small, which explains why there is very little isovector contribution to the fusion barrier.

In summary, we have performed DC-TDHF calculations with the decomposed EDF into isoscalar and isovector parts with the purpose of identifying the isovector contribution to the overall fusion potential barrier. The isovector contribution is an indicator of the influence of particle transfer during the early stages of nuclear contact prior to fusion. We observed that for the $^{40}\text{Ca} + ^{176}\text{Yb}$ system the neutron transfer is from the target to projectile, which leads to the reduction of the potential barrier, whereas for the neutron rich systems the transfer reverses direction and leads to the enhancement of the potential barrier. These changes affect both the height and the width of the barrier. We also observe that transfer does depend on the orientation of the deformed target.

This work was supported by the U.S. Department of Energy under Award No. DE-SC0013847 (Vanderbilt University). In addition, R.G. acknowledges support from a Fisk-Vanderbilt Master's-to-Ph.D. Bridge Program fellowship.

[1] B. B. Back, H. Esbensen, C. L. Jiang, and K. E. Rehm, Recent developments in heavy-ion fusion reactions, *Rev. Mod. Phys.* **86**, 317 (2014).

[2] G. Montagnoli and A. M. Stefanini, Recent experimental results in sub- and near-barrier heavy-ion fusion reactions, *Eur. Phys. J. A* **53**, 169 (2017).

- [3] G. Montagnoli and A. M. Stefanini, Recent experimental results in sub- and near-barrier heavy ion fusion reactions (2nd edition), *Eur. Phys. J. A* **59**, 138 (2023).
- [4] K. Hagino, N. Rowley, and A. T. Kruppa, A program for coupled-channel calculations with all order couplings for heavy-ion fusion reactions, *Comput. Phys. Commun.* **123**, 143 (1999).
- [5] K. Hagino and N. Takigawa, Subbarrier fusion reactions and many-particle quantum tunneling, *Prog. Theor. Phys.* **128**, 1061 (2012).
- [6] K. Hagino, K. Ogata, and A. M. Moro, Coupled-channels calculations for nuclear reactions: From exotic nuclei to superheavy elements, *Prog. Part. Nucl. Phys.* **125**, 103951 (2022).
- [7] A. S. Umar and V. E. Oberacker, Heavy-ion interaction potential deduced from density-constrained time-dependent Hartree-Fock calculation, *Phys. Rev. C* **74**, 021601(R) (2006).
- [8] C. Simenel and A. S. Umar, Heavy-ion collisions and fission dynamics with the time-dependent Hartree-Fock theory and its extensions, *Prog. Part. Nucl. Phys.* **103**, 19 (2018).
- [9] A. B. Balantekin, J. Carlson, D. J. Dean, G. M. Fuller, R. J. Furnstahl, M. Hjorth-Jensen, R. V. F. Janssens, B.-A. Li, W. Nazarewicz, F. M. Nunes, W. E. Ormand, S. Reddy, and B. M. Sherrill, Nuclear theory and science of the facility for rare isotope beams, *Mod. Phys. Lett. A* **29**, 1430010 (2014).
- [10] W. Loveland, Synthesis of transactinide nuclei using radioactive beams, *Phys. Rev. C* **76**, 014612 (2007).
- [11] C. J. Horowitz, E. F. Brown, Y. Kim, W. G. Lynch, R. Michaels, A. Ono, J. Piekarewicz, M. B. Tsang, and H. H. Wolter, A way forward in the study of the symmetry energy: experiment, theory, and observation, *J. Phys. G: Nucl. Part. Phys.* **41**, 093001 (2014).
- [12] B.-A. Li, Àngels. Ramos, G. Verde, and I. Vidaña, Topical issue on nuclear symmetry energy, *Eur. Phys. J. A* **50**, 9 (2014).
- [13] W.-C. Chen and J. Piekarewicz, Searching for isovector signatures in the neutron-rich oxygen and calcium isotopes, *Phys. Lett. B* **748**, 284 (2015).
- [14] P. Danielewicz, R. Lacey, and W. G. Lynch, Determination of the equation of state of dense matter, *Science* **298**, 1592 (2002).
- [15] M. B. Tsang, Y. Zhang, P. Danielewicz, M. Famiano, Z. Li, W. G. Lynch, and A. W. Steiner, Constraints on the density dependence of the symmetry energy, *Phys. Rev. Lett.* **102**, 122701 (2009).
- [16] N. Chamel and P. Haensel, Physics of neutron star crusts, *Liv. Rev. Relativ.* **11**, 10 (2008).
- [17] G. Shen, C. J. Horowitz, and S. Teige, New equation of state for astrophysical simulations, *Phys. Rev. C* **83**, 035802 (2011).
- [18] C. L. Jiang, K. E. Rehm, B. B. Back, H. Esbensen, R. V. F. Janssens, A. M. Stefanini, and G. Montagnoli, Influence of heavy-ion transfer on fusion reactions, *Phys. Rev. C* **89**, 051603(R) (2014).
- [19] C. L. Jiang, A. M. Stefanini, H. Esbensen, K. E. Rehm, S. Almaraz-Calderon, M. L. Avila, B. B. Back, D. Bourgin, L. Corradi, S. Courtin, E. Fioretto, F. Galtarossa, A. Goasduff, F. Haas, M. M. Mazzocco, D. Montanari, G. Montagnoli, T. Mijatovic, R. Sagaidak, D. Santiago-Gonzalez *et al.*, Fusion reactions of $^{58,64}\text{Ni} + ^{124}\text{Sn}$, *Phys. Rev. C* **91**, 044602 (2015).
- [20] J. F. Liang, J. M. Allmond, C. J. Gross, P. E. Mueller, D. Shapira, R. L. Varner, M. Dasgupta, D. J. Hinde, C. Simenel, E. Williams, K. Vo-Phuoc, M. L. Brown, I. P. Carter, M. Evers, D. H. Luong, T. Ebadi, and A. Wakhle, Examining the role of transfer coupling in sub-barrier fusion of $^{46,50}\text{Ti} + ^{124}\text{Sn}$, *Phys. Rev. C* **94**, 024616 (2016).
- [21] C. Simenel, A. S. Umar, K. Godbey, M. Dasgupta, and D. J. Hinde, How the Pauli exclusion principle affects fusion of atomic nuclei, *Phys. Rev. C* **95**, 031601(R) (2017).
- [22] A. S. Umar, C. Simenel, and K. Godbey, Pauli energy contribution to the nucleus-nucleus interaction, *Phys. Rev. C* **104**, 034619 (2021).
- [23] A. S. Umar and V. E. Oberacker, Time dependent Hartree-Fock fusion calculations for spherical, deformed systems, *Phys. Rev. C* **74**, 024606 (2006).
- [24] K. Hagino, Hot fusion reactions with deformed nuclei for synthesis of superheavy nuclei: An extension of the fusion-by-diffusion model, *Phys. Rev. C* **98**, 014607 (2018).
- [25] K. Hagino and S. Sakaguchi, Subbarrier fusion reactions of an aligned deformed nucleus, *Phys. Rev. C* **100**, 064614 (2019).
- [26] A. S. Umar, V. E. Oberacker, and J. A. Maruhn, Neutron transfer dynamics and doorway to fusion in time-dependent Hartree-Fock theory, *Eur. Phys. J. A* **37**, 245 (2008).
- [27] C. Simenel, Particle transfer reactions with the time-Dependent Hartree-Fock theory using a particle number projection technique, *Phys. Rev. Lett.* **105**, 192701 (2010).
- [28] C. Simenel, D. J. Hinde, R. du Rietz, M. Dasgupta, M. Evers, C. J. Lin, D. H. Luong, and A. Wakhle, Influence of entrance-channel magicity and isospin on quasi-fission, *Phys. Lett. B* **710**, 607 (2012).
- [29] K. Sekizawa, TDHF theory and its extensions for the multi-nucleon transfer reaction: A mini review, *Front. Phys.* **7**, 20 (2019).
- [30] Z. Wu, L. Guo, Z. Liu, and G. Peng, Production of proton-rich nuclei in the vicinity of ^{100}Sn via multinucleon transfer reactions, *Phys. Lett. B* **825**, 136886 (2022).
- [31] S. E. Koonin, K. T. R. Davies, V. Maruhn-Rezwani, H. Feldmeier, S. J. Krieger, and J. W. Negele, Time-dependent Hartree-Fock calculations for $^{16}\text{O} + ^{16}\text{O}$ and $^{40}\text{Ca} + ^{40}\text{Ca}$ reactions, *Phys. Rev. C* **15**, 1359 (1977).
- [32] C. Simenel, Particle-number fluctuations and correlations in transfer reactions obtained using the Balian-Vénéroni variational principle, *Phys. Rev. Lett.* **106**, 112502 (2011).
- [33] A. S. Umar, C. Simenel, and W. Ye, Transport properties of isospin asymmetric nuclear matter using the time-dependent Hartree-Fock method, *Phys. Rev. C* **96**, 024625 (2017).
- [34] A. Wakhle, C. Simenel, D. J. Hinde, M. Dasgupta, M. Evers, D. H. Luong, R. du Rietz, and E. Williams, Interplay between quantum shells and orientation in quasifission, *Phys. Rev. Lett.* **113**, 182502 (2014).
- [35] A. S. Umar, V. E. Oberacker, and C. Simenel, Shape evolution and collective dynamics of quasifission in the time-dependent Hartree-Fock approach, *Phys. Rev. C* **92**, 024621 (2015).
- [36] A. S. Umar, V. E. Oberacker, and C. Simenel, Fusion and quasifission dynamics in the reactions $^{48}\text{Ca} + ^{249}\text{Bk}$ and $^{50}\text{Ti} + ^{249}\text{Bk}$ using a time-dependent Hartree-Fock approach, *Phys. Rev. C* **94**, 024605 (2016).
- [37] K. Sekizawa and K. Yabana, Time-dependent Hartree-Fock calculations for multinucleon transfer and quasifission processes in the $^{64}\text{Ni} + ^{238}\text{U}$ reaction, *Phys. Rev. C* **93**, 054616 (2016).
- [38] L. Guo, C. Shen, C. Yu, and Z. Wu, Isotopic trends of quasifission and fusion-fission in the reactions $^{48}\text{Ca} + ^{239,244}\text{Pu}$, *Phys. Rev. C* **98**, 064609 (2018).

- [39] K. Godbey, A. S. Umar, and C. Simenel, Deformed shell effects in $^{48}\text{Ca} + ^{249}\text{Bk}$ quasifission fragments, *Phys. Rev. C* **100**, 024610 (2019).
- [40] K. Godbey and A. S. Umar, Quasifission dynamics in microscopic theories, *Front. Phys.* **8**, 40 (2020).
- [41] P. D. Stevenson, Mean-field simulations of Es-254+Ca-48 heavy-ion reactions, *Front. Phys.* **10**, 1019285 (2022).
- [42] Y. M. Engel, D. M. Brink, K. Goeke, S. J. Krieger, and D. Vautherin, Time-dependent Hartree-Fock theory with Skyrme's interaction, *Nucl. Phys. A* **249**, 215 (1975).
- [43] J. Dobaczewski and J. Dudek, Time-odd components in the mean field of rotating superdeformed nuclei, *Phys. Rev. C* **52**, 1827 (1995).
- [44] K. Vo-Phuoc, C. Simenel, and E. C. Simpson, Dynamical effects in fusion with exotic nuclei, *Phys. Rev. C* **94**, 024612 (2016).
- [45] K. Godbey, A. S. Umar, and C. Simenel, Dependence of fusion on isospin dynamics, *Phys. Rev. C* **95**, 011601(R) (2017).
- [46] A. S. Umar and V. E. Oberacker, Dynamical deformation effects in subbarrier fusion of $^{64}\text{Ni} + ^{132}\text{Sn}$, *Phys. Rev. C* **74**, 061601(R) (2006).
- [47] A. S. Umar, C. Simenel, and V. E. Oberacker, Energy dependence of potential barriers and its effect on fusion cross sections, *Phys. Rev. C* **89**, 034611 (2014).
- [48] C. Simenel, R. Keser, A. S. Umar, and V. E. Oberacker, Microscopic study of $^{16}\text{O} + ^{16}\text{O}$ fusion, *Phys. Rev. C* **88**, 024617 (2013).
- [49] A. S. Umar, V. E. Oberacker, and C. J. Horowitz, Microscopic sub-barrier fusion calculations for the neutron star crust, *Phys. Rev. C* **85**, 055801 (2012).
- [50] R. Keser, A. S. Umar, and V. E. Oberacker, Microscopic study of Ca + Ca fusion, *Phys. Rev. C* **85**, 044606 (2012).
- [51] V. E. Oberacker, A. S. Umar, J. A. Maruhn, and P. G. Reinhard, Microscopic study of the $^{132,124}\text{Sn} + ^{96}\text{Zr}$ reactions: Dynamic excitation energy, energy-dependent heavy-ion potential, and capture cross section, *Phys. Rev. C* **82**, 034603 (2010).
- [52] X. Jiang, J. A. Maruhn, and S. W. Yan, Configuration transition effect in heavy-ion fusion reactions with deformed nuclei, *Europhys. Lett.* **112**, 12001 (2015).
- [53] A. S. Umar and V. E. Oberacker, Three-dimensional unrestricted time-dependent Hartree-Fock fusion calculations using the full Skyrme interaction, *Phys. Rev. C* **73**, 054607 (2006).
- [54] K.-H. Kim, T. Otsuka, and P. Bonche, Three-dimensional TDHF calculations for reactions of unstable nuclei, *J. Phys. G: Nucl. Part. Phys.* **23**, 1267 (1997).
- [55] A. S. Umar, M. R. Strayer, J. S. Wu, D. J. Dean, and M. C. Güçlü, Nuclear Hartree-Fock calculations with splines, *Phys. Rev. C* **44**, 2512 (1991).
- [56] J. J. Kolata, A. Roberts, A. M. Howard, D. Shapira, J. F. Liang, C. J. Gross, R. L. Varner, Z. Kohley, A. N. Villano, H. Amro, W. Loveland, and E. Chavez, Fusion of $^{124,132}\text{Sn}$ with $^{40,48}\text{Ca}$, *Phys. Rev. C* **85**, 054603 (2012).
- [57] V. E. Oberacker and A. S. Umar, Microscopic analysis of sub-barrier fusion enhancement in $^{132}\text{Sn} + ^{40}\text{Ca}$ versus $^{132}\text{Sn} + ^{48}\text{Ca}$, *Phys. Rev. C* **87**, 034611 (2013).